Int J Fract (2013) 181:67–81
DOI 10.1007/s10704-013-9821-8

ORIGINAL PAPER

Non-uniqueness of cohesive-crack stress-separation law of human and bovine bones and remedy by size effect tests

Kyung-Tae Kim · Zdeněk P. Bažant · Qiang Yu

Received: 27 July 2012 / Accepted: 15 February 2013 / Published online: 3 April 2013

Abstract It is shown that if the bilinear stress-separation law of the cohesive crack model is identified from the complete softening load-deflection curve of a notched human bone specimen of only one size, the problem is ill-conditioned and the result is non-unique. The same measured load-deflection curve can be fitted with values of initial fracture energy and tensile strength differing, respectively, by up to 100 and 72.4 % (of the lower value). The material parameters, however, give very different load-deflection curves when the specimen is scaled up or down significantly. This implies that the aforementioned non-uniqueness could be avoided by testing human bone specimens of different sizes. To demonstrate it, tests of notched bovine bone beams of sizes in the ratio of $1{:}\sqrt{6}{:}6$ are conducted. To minimize random scatter, all the specimens are cut from one and the same bovine bone, even though this limits the number of specimens to 8. A strong size effect is found, but an anomaly in the size effect data trend is obtained, probably due to random scatter and too small a number of specimens. Further it is shown that the optimum range of size effect testing based on Bažant's size effect law approximately coincides with the size range of beams that can be cut from one bovine bone. By size effect fitting of previously published data on human bone, it is shown that the optimum size range calls for beam depths under 10 mm, which is too small for the standard equipment of mechanics of materials labs and would require a special miniaturized precision equipment.

Keywords Scaling · Strength · Fracture energy · Quasibrittle failure · Nonlinear fracture mechanics · Orthotropic materials · Bio-materials

Z. P. Bažant (✉)
Northwestern University, 2145 Sheridan Rd. A123,
Evanston, IL, USA
e-mail: z-bazant@northwestern.edu

K.-T. Kim
Northwestern University,
2145 Sheridan Road, CEE Evanston, IL 60201, USA
e-mail: ktkim1@gmail.com

Present Address:
K.-T. Kim
Samsung Techwin R&D Center, Bundang-gu,
Seongnam-si, Gyeonggi-do 463-400,
Republic of Korea
e-mail: KT2.Kim@samsung.com

Q. Yu
Department of Civil and Environmental Engineering,
Swanson School of Engineering, University of Pittsburgh,
Pittsburgh, PA 15261, USA
e-mail: qiy15@pitt.eduu

1 Introduction

Bone fracture used to be modeled in terms of linear elastic fracture mechanics (LEFM), in which the fracture process zone (FPZ) is considered to be a point and the material fracture properties are characterized by a single parameter, the fracture energy G_F or, equivalently, by fracture toughness $K_{Ic} = \sqrt{E_{ef} G_F}$ (where E_{ef} = effective elastic modulus of orthotropic

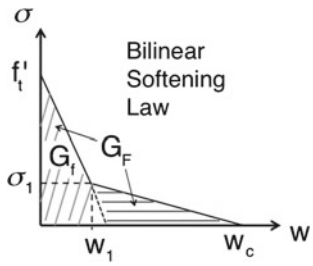

Fig. 1 Illustration of bilinear law parameters; G_f, initial fracture energy, G_F, total fracture energy, σ_1, knee stress and f_t', tensile strength

material, see "Appendix I"). Recently, it has been convincingly demonstrated that LEFM is inadequate and that nonlinear fracture mechanics must be used (Nalla et al. 2005, 2004). In these studies it was concluded that the observed FPZ size in human cortical femur bone is roughly 5 mm, which is far from negligible compared to the bone dimensions. For fracture characterization, Yang et al. (2006a,b) adopted the cohesive crack model, which is a well proven model for all quasibrittle (or heterogeneous brittle) materials.

The cohesive crack model is the limiting case of the crack band model (Bažant and Oh 1983), a model which reflects more realistically the fact that the FPZ has a finite width h. For isolated cracks, and for the opening mode of fracture, both models are virtually equivalent if the normal strain across the crack band (or the FPZ) is taken as the average, $\epsilon = w/h$. The crack band model is a generalization of the cohesive crack model which is more powerful in the sense that it can take into account the effect of normal stress and shear stresses acting parallel to the crack. But for the standard notched fracture tests these stresses are too small to matter.

For most practical purposes, the cohesive stress-separation law can be idealized as bilinear (Fig. 1). It is characterized by 4 parameters: The total and initial fracture energies G_F and G_f, representing the areas under the complete stress-separation curve and under the initial descending segment extended to zero stress; the tensile strength, f_t', giving the stress at which the softening begins; and the stress σ_1 at the so-called "knee" point, at which the slope suddenly decreases.

It must be emphasized that the proper way to determine the tensile strength limit f_t' of the cohesive crack model is by fracture tests. This strength limit f_t' need not be, and generally is not, the same as the tensile strength obtained by the conventional direct tension, flexural or split-cylinder tests. One reason is the fact that, in the case of quasibrittle materials, the tensile strength obtained from these conventional tests exhibits a strong size effect.

For measuring G_F, the work-of-fracture method, introduced first for ceramics (Nakayama 1965; Tattersall and Tappin 1966) and later pioneered for concrete by Hillerborg et al. (1976) and Petersson (1981), has become popular and was standardized for concrete by RILEM (1990). In this method, $G_F \approx W_f/A$ where W_f = area under the measured load-deflection curve and A = area of the entire broken ligament (Bažant and Planas 1998). The ratio G_F/G_f varies widely—for concrete roughly from 2 to 6. The results delivered for concrete by this method have been very scattered, with the coefficient of variation of G_F more than twice as large as that of G_f measured by the size effect method (Bažant and Becq-Giraudon 1999).

In Bažant and Yu (2011), it was noted that this high scatter must have been caused mainly by the inherent non-uniqueness in identifying the cohesive crack model from concrete specimens of one size only, due to ill-conditioning of the data fitting problem. It was found that the same complete load-deflection curve can be matched closely by cohesive laws in which the strength limit f_t' differs by 71 % and the initial G_f by 55 % (of the lowest value). Further it was shown that, for concrete, this ambiguity can be eliminated by testing the load-deflection curves of specimens of significantly different sizes.

To explore this idea for bone is the main objective of this study, which will build mainly on the results of Yang et al.'s (2006a, b) tests of human bone. Limited tests of the size effect in bone, made on bovine bone, will also be reported and discussed.

2 Non-uniqueness problems in identification of fracture parameters of human bone

Yang et al. (2006a,b) reported tests of three compact tension specimens giving three curves of the load versus the crack mouth opening displacement (δ_{CMOD}), which were rather close to each other. The dimensions of the specimens used differed by <6 %, which means that there was almost no size effect. The reported orthotropic elastic properties of the bone were E_1 = 16 GPa, E_3 = 12 GPa, G_{31} = 1.5 GPa, ν_{31} = 0.225 and ν_{13} = 0.3 (see "Appendix I"). Yang et al. fitted

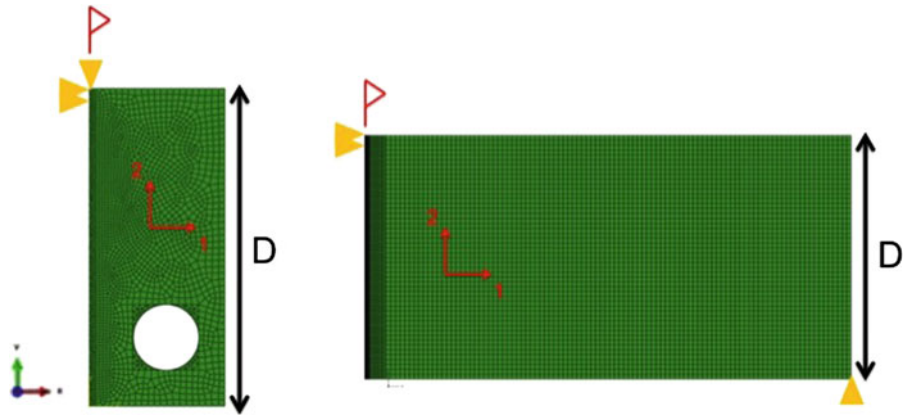

Fig. 2 Geometry of numerical simulation: compact tension test for human bone (*Left*) and three-point-bending test for bovine femur (*Right*)

their measured load-δ_{CMOD} curves by finite elements, and obtained a good fit, shown in Fig. 11. They used the cohesive crack model with the softening bilinear stress-separation law (their Fig. 8) defined by parameters:

$$f_t' = 60 \text{ MPa}, \quad \sigma_1 = 30 \text{ MPa}, \quad G_f = 0.72 \text{ kJ/m}^2, \quad G_F = 1.44 \text{ kJ/m}^2 \tag{1}$$

(in Yang et al.'s notation, $G_F = W_{tip} + W_{brid}$ and $W_{tip} = G_f$)

When the cohesive traction-separation law of the material is given, the load-displacement curves of notched specimens with growing cohesive cracks can be effectively computed by the procedure described in Bažant and Planas (1998), p. 190. In this procedure, the specimen is discretized by finite elements, in which the orthotropy of bone is taken into account (Fig. 2). Then all the interior displacements are condensed out. What remains is an influence matrix relating only the nodal forces and displacements $v_i \delta_i (i = 1, 2, \ldots N)$ at all the crack face nodes and displacement w at the load point. Four conditions must be imposed: 1) $\sigma = 0$ in the notch; 2) $\sigma = f(w)$ inside the cohesive zone (representing the FPZ); and 3) $v = 0$ over the rest of the ligament; and 4) vanishing total stress intensity factor K_I at the tip of the cohesive crack.

Setting the displacements v_i at each crack face node equal to the displacement corresponding to the crack-bridging stress σ according to the inverse of the traction-separation law $\sigma = f(w)$, one gets as many equations as there are unknown displacements. The opening displacement at the crack mouth node is incremented in small steps. By solving the system of linear equations for unknown displacement increments, the equilibrium values of load P, load-point displacement w, and nodal crack openings displacements v_i are obtained. This yields the load-displacement curve $P(w)$, from which the maximum load is identified.

To check for uniqueness in fitting the measured load-displacement curve, the bilinear law $\sigma = f(v)$ has been varied while trying to maintain a good fit. This effort led to three $f(v)$ curves that are shown in Fig. 11a and are characterized by the following parameter sets:

$$\text{Set 1: } f_t' = 115 \text{ MPa}, \ \sigma_1 = 23 \text{ MPa}, \ G_f = 0.6 \text{ kJ/m}^2, \ G_F = 1.2 \text{ kJ/m}^2 \tag{2}$$

$$\text{Set 2: } f_t' = 100 \text{ MPa}, \ \sigma_1 = 30 \text{ MPa}, \ G_f = 0.6 \text{ kJ/m}^2, \ G_F = 1.2 \text{ kJ/m}^2 \tag{3}$$

$$\text{Set 3: } f_t' = 120 \text{ MPa}, \ \sigma_1 = 24 \text{ MPa}, \ G_f = 0.2 \text{ kJ/m}^2, \ G_F = 1.0 \text{ kJ/m}^2 \tag{4}$$

Among these stress-separation curves, the maximum difference in G_f is 72.4 % and in f_t' is 100 %, which is enormous; Fig. 11b. Nevertheless, the differences among the load-δ_{CMOD} curves corresponding to these three parameter sets are negligible compared to the inevitable experimental scatter (Yang et al. 2006a). All these three different stress-separation curves give about equally good fits of the load-displacement curve measured by Yang et al. It must be concluded that the bilinear softening stress-separation curve of the cohesive crack model cannot be uniquely identified from tests of one size only.

A similar non-uniqueness has already been shown for concrete, albeit for different shapes of the bilinear softening curve (Bažant and Yu 2011).

It has been demonstrated that the different bilinear softening curves giving a close fit of the same load-deflection diagram can be distinguished by the size effect, on which we focus now.

2.1 Review of size effect of cohesive fracture

In theories in which failure is decided solely by material strength, i.e., a critical value of stress (or strain, or both), as in the case of elasticity and plasticity, the nominal strength of geometrically similar specimens or structures

$$\sigma_N = P_{max}/bD \tag{5}$$

is independent of the structure size D (or dimension); here P_{max} = maximum load, and b = structure width. Because only relative changes of D matter, any structural dimension can be adopted as the characteristic size, although for beams the beam depth is customary. If the failure criterion involves energy per unit area, or some material characteristic length, σ_N of geometrically similar structures decreases with D. This came to be called the size effect. According to LEFM, $\sigma_N \propto D^{-1/2}$ (if the notches or cracks are similar), and so the size effect plot of $\log \sigma_N$ versus $\log D$ is a straight line of slope $-1/2$. For quasibrittle materials, the size effect is intermediate between the strength theory (no size effect) and LEFM (the maximum possible size effect), and the size effect plot represents a gradual transition from the horizontal asymptote of strength theory to an inclined asymptote of slope $-1/2$ (Fig. 6a).

The size effect in specimens or structures that either have a notch or exhibit a stable growth of a large crack prior to maximum load approximately follows the size effect law (SEL of Type 2), given by one of the following alternative expressions (Bažant and Planas 1998; Bažant 1984, 1997; Bažant and Kazemi 1990, 1991):

$$\sigma_N = \frac{Bf_t'}{\sqrt{1 + D/D_0}} = \sqrt{\frac{E_{ef}G_f}{g'(\alpha_0)c_f + g(\alpha_0)D}} \tag{6}$$

Here f_t' = tensile strength, D_0 = transitional size, which is a constant depending on structure geometry, c_f = material length constant roughly equal to one half of the FPZ length; $B = \sqrt{l_{ch}/c_f g_0'}$, which is a dimensionless geometry-dependent parameter; a_0 = notch depth equivalent to initial crack length, $a = a_0 + c$ = total crack length, $\alpha = a/D$, $\alpha_0 = a_0/D$, c_f = length of the FPZ when it begins to move away from the notch tip (considered to be a material property); $g(\alpha_0) = k_0^2$ = initial dimensionless LEFM energy release rate, $g'(\alpha_0) = 2k_0(\alpha_0)k_0'(\alpha_0)$ and $k(\alpha_0)$ = initial dimensionless stress intensity factor; and K_I = LEFM stress intensity factor. According to the size effect law (Bažant and Planas 1998; Bažant and Kazemi 1991; Bažant 2005),

$$c_f = D_0 \frac{g(\alpha_0)}{g'(\alpha_0)}, \quad G_f = (Bf_t')^2 g(\alpha_0)\frac{D_0}{E_{ef}} \tag{7}$$

Equation (6) has been derived in several different ways (Bažant and Planas 1998; Bažant 2005). It represents an energetic size effect, reflecting the fact that, at fixed σ_N, the energy release rate of the crack would increase with D faster than the energy dissipation rate. The Weibull statistical size effect is absent from specimens containing notches or large cracks formed stably before reaching the maximum load.

2.2 Differences in size effects for various stress-separation laws of human bone

It is now interesting to use the foregoing three parameter sets in Eq. (2) to compute the load-deflection curves, imagining the specimens of Yang et al. to be scaled up by a factor of 4. The results, presented in Fig. 12, indicate that the computed maximum loads for these sets become very different. They differ by as much as 29 % (of the lower value).

It follows that, if the measured load-deflection curve is supplemented by size effect data, different cohesive softening bilinear laws can be distinguished.

2.3 Differences in maximum loads of human bones of different sizes

It is now interesting to use the foregoing three parameter sets in Eq. (2) to compute the load-deflection curves, imagining the specimens of Yang et al. to be scaled up by a factor of 4. The results, presented in Fig. 12, indicate that the computed maximum loads for these sets become very different. They differ by as much as 29 % (of the lower value).

It follows that, if the measured load-deflection curve is supplemented by size effect data, different cohesive softening bilinear laws can be distinguished.

2.3.1 Fracture tests of bone at different sizes

Is it possible to conduct size effect tests of bone? The aforementioned specimens of human bone scaled up

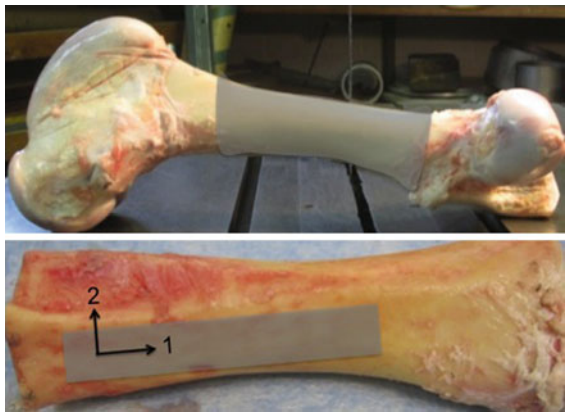

Fig. 3 Raw bovine femur and location of specimens with orientation

by a factor of 4 would in fact be impossible to carry out because the bone cross section is not large enough for cutting such enlarged specimens.

For human bone, only a modest upward scaling of Yang et al.'s tests is possible. Therefore, a significant down-scaling, which would result in miniature specimens, with beams of millimeter-range depths, would be required and would necessitate a special testing device.

The bovine femurs, on the other hand, are sufficiently larger than the human ones to allow producing specimens of sufficiently different sizes, testable with standard equipment of civil or mechanical engineering labs.

A femur bone from a 6 month old cow was purchased from a biological research facility (Research 87 Inc., Boylston, MA). To obtain consistent results, all the specimens were cut from the cortical part of the bone. Because of the orthotropy of bone (Van Buskirk et al. 1981), all the long sides of specimens were cut along the fiber orientation (Fig. 3). A low-speed diamond blade was used to allow precision cuts while minimizing material damage from frictional heating. After cutting and until the time of test, the bone specimens were preserved in Hanks' balanced salt solution (HBSS) at 4 °C. The tests were performed at room temperature. Since they were moved to the testing room just before the test, no further moisturizing of the specimens was made during the tests.

To minimize random scatter, all the specimens had to be cut from one and the same bone. Of course, this limited the scope of testing, since cutting of further specimens would have required using another bone, which would inevitably have had somewhat different properties.

It was nevertheless possible to cut the total of 8 specimens from one piece of cortical bone; see Fig. 3. All the specimens were notched three-point bend beams of three sizes, geometrically scaled in two dimensions while keeping a constant width $b = 4$ mm (Fig. 4).

The size ratio was $1{:}\sqrt{6}{:}6$, and the depth of the largest specimens was $D = 18$ mm, which was the maximum achievable (Table 1). Although as many beams as possible were cut from the cortical part of one and the same bone, their number was still relatively small by the standards of fracture testing of quasibrittle materials, in which significant random scatter is inevitable.

The tests were conducted in a standard closed-loop servo-controlled (MTS) testing machine. All the specimens failed in a similar way, before onset of open crack growth from the notch, and the observed paths of cracks growing during post-peak softening were similar, roughly in straight extension from the notch. Because of viscoelastic behavior of the bone, the loading rates were selected to reach the peak load for all the sizes within about the same time, which was about 1,000 s. To achieve stable response in the postpeak softening range, the large and medium specimens were

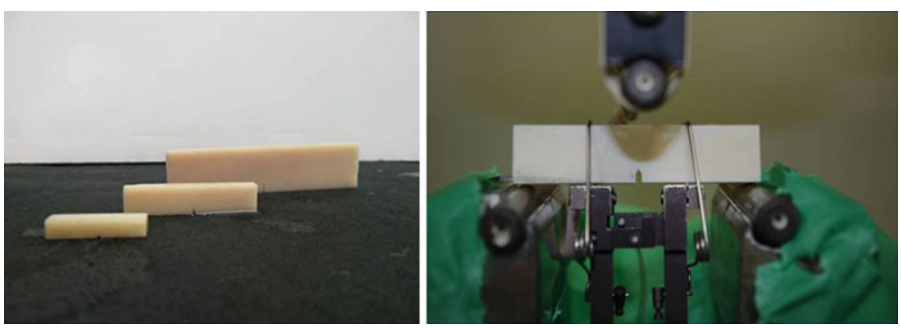

Fig. 4 Geometrically similar specimens of bovine cortical femur ($1{:}\sqrt{6}{:}6$) (*Left*) medium specimen during δ_{CMOD} controlled test (*Right*)

Table 1 Bone specimen specifications and peak loads

Specimen	L (mm)	D (mm)	b (mm)	a_0 (mm)	Peak loads (N)
L-1	72	18	4	3.6	992.2
L-2	72	18	4	3.6	790.6
M-1	29.4	7.35	4	1.47	400.4
M-2	29.4	7.35	4	1.47	400.1
M-3	29.4	7.35	4	1.47	420.7
S-1	12	3	4	0.6	217.6
S-2	12	3	4	0.6	217.0
S-3	12	3	4	0.6	216.4

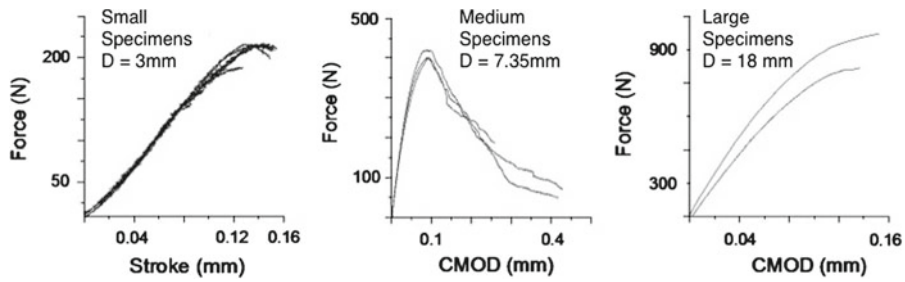

Fig. 5 Test results of load-displacement curves of bovine femur

loaded at constant velocity controlled by a crack-mouth opening displacement (CMOD) gauge. Since a short enough gauge was not available for the smallest specimens, their loading was controlled by the load-point displacement rate, which meant that these specimens lost stability right after the peak and the postpeak curve could not be measured. Nevertheless, the maximum (peak) loads could be recorded for all the specimens.

In total, 2 specimens of the largest size, 3 of the medium size and 3 of the smallest size were tested. The test results are shown in Table 1. The data points plotted in Fig. 6a represent the peak loads of all the specimens tested. The solid curves in Fig. 5 show the actual load-deflection curves of the individual specimens of each size, obtained in these test.

Looking at Fig. 6, one can immediately make five observations:

1. The overall mean slope of the data trend confirms that there is indeed a size effect, and that the size effect is transitional between the LEFM (slope $-1/2$) and the strength theory (slope 0). As $D \to \infty$, the FPZ would shrink to zero size (or a point) relative to D, and so the slope $-1/2$ of LEFM, shown as the dashed line, must be approached. When $D \to 0$, the entire cross section is fully occupied by the cohesive zone and so the plot should approach the horizontal asymptote of plasticity (Bažant 2005). For quasibrittle materials, such transitional size effect is a salient feature, and its presence implies that the cohesive softening fracture model is applicable.
2. While the size effect law for quasibrittle materials gives, in the log-log plot of Fig. 6, a curve of increasing slope (i.e., convex curvature), the data points indicate a decreasing slope (i.e. concave curvature). So the test results do not support the size effect law (Eq. 6).
3. At the same time, however, it must be noted that, in view of the large random scatter known to occur in fracture testing of quasibrittle materials, the number of tests is too small to expect a close agreement with the size effect law. Therefore, the observed decreasing, rather than increasing, slope of the data trend (i.e., convex rather than concave) is most likely a manifestation of random scatter. The scatter is likely caused by the fact that different parts of the bovine cortical bone do not have the same properties.
4. Would it help to increase the number of tests, to reduce the scatter? A modest increase would probably not help because the additional specimens would have to be cut from different bones. This would

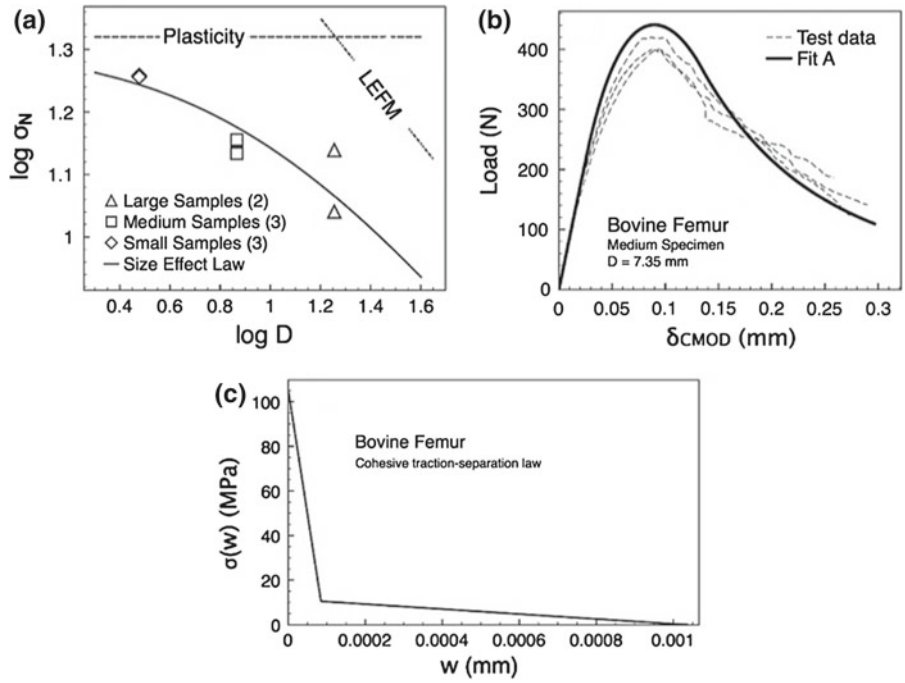

Fig. 6 **a** Size effect data fitting using Levenberg–Marquadt algorithm **b** fitting cohesive crack model simulation to load-δ_{CMOD} of medium specimen **c** unique bilinear law that matches both size effect data and postpeak curves

inevitably introduce higher scatter since different bones always have different properties. A further increase in the number of specimens would require using bones from different cows, which would further magnify the scatter (the problem is similar to the testing of concrete specimens cast either from one batch of concrete or from different batches of supposedly the same concrete, which never have the same properties).

5. Only the statistics of tests of a very large number of specimens, from many cows, would be likely to produce a clear trend, in the mean sense. Such tests should be carried out in the future.

In view of the five foregoing points, it does make sense to interpret the bovine fracture tests in terms of the size effect law, Eq. (6), in spite of the convex trend of data points (Fig. 6). So the size effect law is optimally fitted to the data using Levenberg–Marquardt nonlinear optimization algorithm. The fitting yields the following size effect law parameters:

$$Bf_t' = 132 \text{ MPa}, \quad D_0 = 8.81 \text{ mm} \tag{8}$$

Then, the size effect law is used to provide the fracture energy and the effective length of the FPZ, using the following relationships:

$$G_f = \frac{(Bf_t')^2}{(c_N)^2 E_{ef}} D_0 g(\alpha_0), \quad c_f = \frac{g(\alpha_0)}{g'(\alpha_0)} \tag{9}$$

The dimensionless energy release function $g(\alpha_0)$ for the orthotropic material properties of bone has the form: $g(\alpha) = \alpha\left\{(1.900 - \alpha[-0.089 + 0.603(1-\alpha) - 0.441(1-\alpha)^2 + 1.223(1-\alpha)^3])^2/((1+2\alpha)^2 (1-\alpha)^3)\right\}$. This gives, for the present specimen geometry, $g(0.2) = 0.612$, $g'(0.2) = 3.41$ (see "Appendix I"). Then, matching the two expressions in Eq. 6 and using the aforementioned expressions for G_f and c_f in terms of Bf_t' and D_0, one gets the estimates

$$G_f \approx 4.95 \text{ kJ/m}^2, \quad c_f \approx 1.58 \text{ mm} \tag{10}$$

Note also that c_f is proportional to Irwin's characteristic length $l_{ch} = E' G_f / f_t'^2$.

At the peak loads of typical fracture specimens, the cohesive stresses (or tractions) at all or nearly all of the points of the FPZ still remain within the initial steep segment of the bilinear stress-separation law. Therefore, the fracture energy provided by the size effect tests is the initial fracture energy G_f. No information can be obtained on G_F since its value also depends on the tail segment of the bilinear law, which is yet not entered by the bone when the specimen is at the peak load.

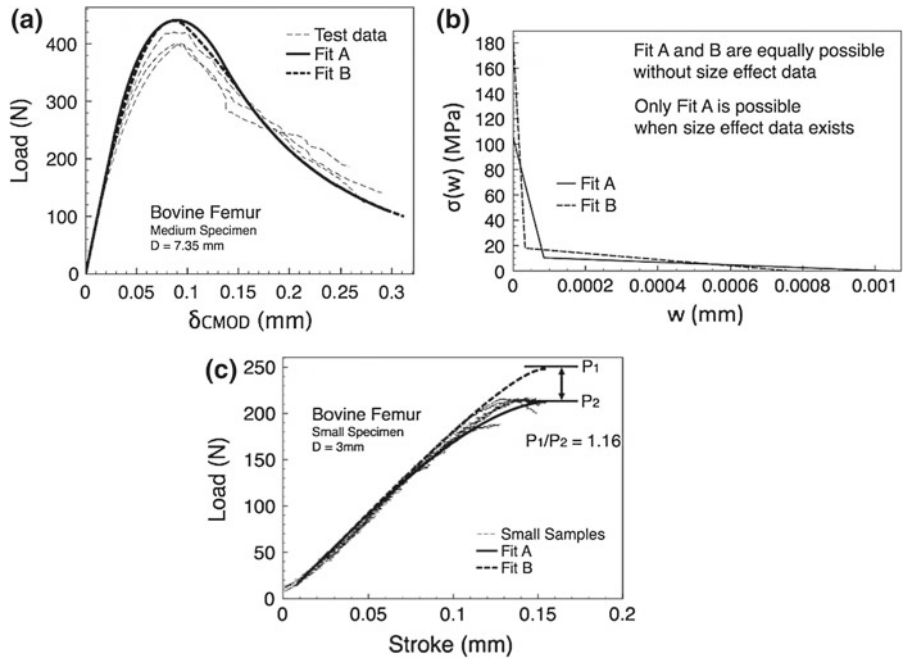

Fig. 7 Missing size effect data cause bilinear laws to be ill-conditioned; **a** post peak curves can be closely matched by two different bilinear softening laws **b** two bilinear laws exhibit f_t' and G_f differed by 71 and 55 % respectively. **c** difference in peak loads corresponding to two cohesive softening laws

2.4 Non-uniqueness of bovine fracture parameters identified from load-displacement curve of one size only

As pointed out in Cusatis and Schauffert (2009), and Yu et al. (2010), the linear size effect plot (Eq. 13 below) is unique only for a fixed shape of the cohesive softening stress-separation law. For $G_F/G_f = 2$ and $\sigma_1/f_t' = 0.1$, finite element simulations show that the $\bar{Y}$-intercept of the intermediate asymptote is $\gamma = 0.72$ and of the final asymptote is 2.5. The ratio of the slopes of these asymptotes is $\chi = G_F/G_f = 2$ (Fig. 9).

Consider now the load-δ_{CMOD} curve for only one medium size specimen of bovine bone (Fig. 5). Fitting by Levenberg–Marquardt nonlinear optimization algorithm showed that this curve can be closely matched (see Fig. 7a) by the following two sets of bilinear fracture parameters:

$$\text{Set 1:}\quad f_t' = 180\ \text{MPa},\quad G_f = 3.30\ \text{kJ/m}^2,\quad G_F/G_f = 3,\quad \sigma_1/f_t' = 0.1 \tag{11}$$

$$\text{Set 2:}\quad f_t' = 105\ \text{MPa},\quad G_f = 4.95\ \text{kJ/m}^2,\quad G_F/G_f = 2,\quad \sigma_1/f_t' = 0.1 \tag{12}$$

The difference between these two sets is 71 % in tensile strength f_t and 55 % in the initial fracture energy, G_f (relative to the lower value). At the same time, the difference in the corresponding load–δ_{CMOD} curves is negligible and much smaller than the inevitable experimental scatter.

2.5 Optimal size range for size effect tests

For bilinear softening cohesive laws there exists a certain optimal size range in which the size effect testing gives very accurate results. For concrete, this range happens to coincide with the convenient size range of laboratory tests. Is the convenient size range for bone also the optimal size range? Before answering this question, this concept needs to be explained at least briefly.

The easiest way to fit the SEL to test data is to convert Eq. 6 to a linear regression equation, which has the form $Y = AX + C$ where $X = D$, $Y = \sigma_N^{-2}$, $A = g_0/EG_f$, $C = g_0' c_f/EG_f$ where $g_0 = g(\alpha_0)$ and $g_0' = [\mathrm{d}g(\alpha)/\mathrm{d}\alpha]_{\alpha=\alpha_0}$ (Bažant and Planas 1998; Bažant 1997; Bažant and Kazemi 1990). The length constant $c_f = \gamma l_1$ where $l_1 = EG_f/f_t'^2 =$ Irwin-type material characteristic length (Irwin 1958) which is, however, defined on the basis of G_f rather than the usual G_F.

To clarify the relation of the cohesive crack model to the size effect law, it is convenient to rearrange the equation $Y = AX + C$ into a different linear plot having the

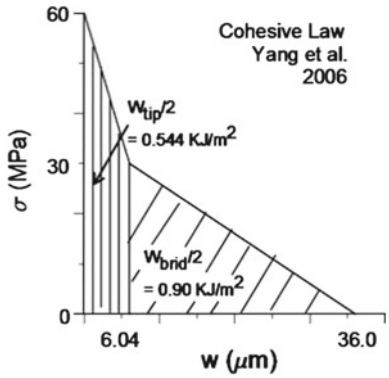

Fig. 8 Bilinear parameters defined in Yang et al.

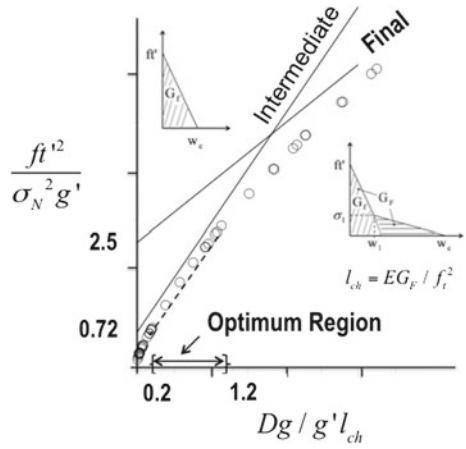

Fig. 9 Size effect law related to cohesive crack model

slope of 1 (Bažant and Yu 2011; Cusatis and Schauffert 2009; Yu et al. 2010);

$$\frac{f_t'^2}{g_0'\sigma_N^2} = \frac{c_f}{l_1} + \frac{g_0 D}{g_0' l_1} \quad \text{or} \quad \bar{Y} = \gamma + \bar{D} \tag{13}$$

where $\bar{Y} = f_t^2/g_0'\sigma_N^2$, $\bar{D} = g_0 D/g_0' l_1$. The $\bar{Y}$-intercept γ varies with the shape of the bilinear law, but only little (note that g_0 is nonzero because the initial relative crack length α_0 is the initial relative notch length which is non-zero).

In the case of bilinear softening, this regression equation may be characterized by two asymptotes: intermediate and final. The intermediate asymptote (intermediate in the sense of Barenblatt 1959, 1962) would be approached infinitely closely if the tail segment of the bilinear stress-separation curve did not exist. The final asymptote is approached when the cohesive stresses in the FPZ enter far into the tail segment already at the maximum load. According to finite element simulations, the stresses in all of the FPZ lie, at maximum load, on the first linear segment of the bilinear law if $\bar{D} \leq 10$.

Numerical simulations show that the cohesive stresses at maximum load enter the second linear segment of the cohesive softening law only if $\bar{D} > 10$. In the case of bone, the second linear segment is, at maximum load, never probed because the size $\bar{D} = 10$ is much larger than the feasible size of laboratory specimens of bone, as well as concrete (and rock, fiber composites, etc.).

Therefore, it is impossible to identify the G_F-value from size effect tests of feasible size.

But in computations the specimen size can be scaled up without limits as desired. The computed results can approach the final asymptote of the size effect plot closely enough (Fig. 8).

When the region ($\bar{D} \leq 2$) is zoomed at (Fig. 9), one should note that there is an extended segment that is parallel to the intermediate asymptote. This convenient property, which makes accurate determination of G_f possible, would not exist if the plot of $\bar{Y}$ versus $\bar{D}$ did not have to transit to the final asymptote of a smaller slope. Obviously, the size effect testing gives the most accurate results when conducted in this segment (Cusatis and Schauffert 2009; Yu et al. 2010).

For concrete, computations showed this segment to be $\bar{D} \in (0.4, 1.4)$. While this size range would suffice for materials with low scatter such as aluminum, it is too narrow for materials such as concrete for which the test results have a high scatter. For concrete, accuracy demands the size range ≥8:1. To achieve it, the range of testing was extended symmetrically on both sides of the straight segment. This kind of extension preserves the same slope of the regression line, which is what matters for G_f, and reduces somewhat the $\bar{Y}$-intercept. For concrete, the testing range with this property was found to be $\bar{D} \in (0.2, 1.8)$ (Yu et al. 2010, Figs. 5–7), which causes γ to decrease to 0.28.

For bovine femur, the present size range of 1:6 appears to be sufficient, and it also seems the maximum achievable. Based on the simulation results in Fig. 9, the dimensionless optimum size range for bone is determined as

$$\bar{D} \in (0.2, 1.2) \tag{14}$$

This optimum range is obtained by setting $\sigma_1/f_t' = 0.1$ and $G_F/G_f = 2$.

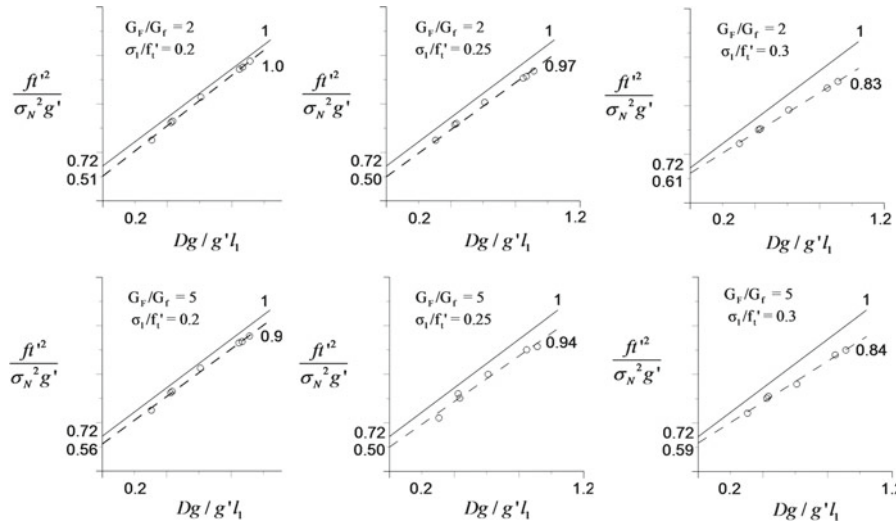

Fig. 10 Different G_F/G_f and σ_1/f_t' studied to determine optimum testing range

Table 2 Effect of G_F/G_f on the optimal range and extended range

	$\sigma_1/f_t' = 0.2$		$\sigma_1/f_t' = 0.25$		$\sigma_1/f_t' = 0.3$	
$\bar{D}$	Slope	γ	Slope	γ	Slope	γ
$G_F/G_f = 2$						
0.2–1.2	1.04	0.51	0.97	0.50	0.83	0.61
0.15–1.25	1.27	0.26	1.21	0.28	1.12	0.30
$G_F/G_f = 5$						
0.2–1.2	0.98	0.56	0.94	0.50	0.84	0.59
0.15–1.25	1.27	0.26	1.18	0.29	1.01	0.32

Does the dimensionless optimum size range depend on the shape of the cohesive softening curve? In this regard, only knee stress values $<0.25 f_t'$ and G_F/G_f values <5 need to be considered, higher ones being unreasonable (in analogy with the studies of concrete Rokugo et al. 1989). To clarify the effect of knee stress, σ_1/f_t' is increased from 0.2 to 0.3 while $G_F/G_f = 2$. Then the slope and the γ values are compared. In Fig. 10, for $\sigma_1/f_t' < 0.25$, the slopes are virtually parallel to 1 and the γ-values are close to each other, approximately equal to 0.5. Furthermore, in this range, the effect of total fracture energy G_F seems negligible. When G_F/G_f is changed to 5, the slopes are still close to 1 and $\gamma \approx 0.53$. Nevertheless, both G_F/G_f ratios give significant errors when $\sigma_1/f_t' = 0.3$. In this case, the calculated G_f and f_t' values vary by as much as 17 and 20 %, respectively. From these observations, it is concluded that the optimum range of (0.2, 1.2) is not much affected by changing the shape of the bilinear law (provided that $\sigma_1/f_f' < 0.25$); see Table 2.

To check whether further expansion of the optimum range is possible, the range was extended on both sides to (0.15, 1.25), and σ_1/f_t' and G_F/G_f were varied again. Unlike the previous results, the errors seem significant even for $\sigma_1 < 0.25 f_t'$, with G_f differing by at least 21 %. A change in the total fracture energy does not help to reduce the error. Even when $G_F/G_f = 5$ the error is at least 18 %, while γ is surprisingly consistent, close to 0.27. But 0.27 is almost 50 % lower than the previous result. In all cases, neither f_t' nor G_f is reliable in the extended range.

When the dimensionless optimum range is converted to the real scale, it becomes approximately $D \in$ (4, 24 mm). It is fortunate that it coincides with the convenient range of laboratory tests of bovine femur.

As a result, the size effect law of Eq. 6 may be written as

$$\frac{1}{\sigma_N^2} = \frac{g_0}{f_t'^2 l_1} D + 0.518 \frac{g_0'}{f_t'^2} \tag{15}$$

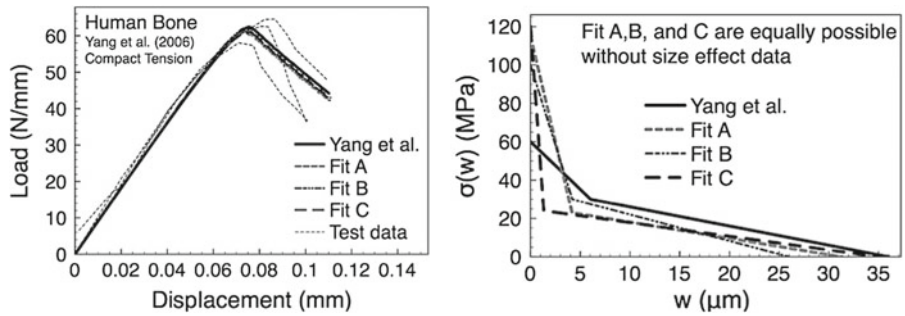

Fig. 11 Three different cohesive softening laws $\sigma(w)$ (*Fit A*, *B*, and *C*) giving the same load-displacement curves

This equation allows optimal direct identification of f_t' and l_1 of bone from the size effect measurements, upon which $G_f = l_1 f_t'^2 / E_{ef}$.

Which test should be used to determine f_t' for the cohesive crack model? Based on one study (Guinea et al. 1992) for concrete, it was thought to be the Brazilian splitting test of cylinders of diameter 6 in. But later studies revealed a problem—the strength identified from the splitting test is markedly size dependent and the size dependence varies with the concrete type.

2.6 Remedy of non-uniqueness for bovine bone specimens

As demonstrated for bovine femur, the values of G_f and f_t' for the softening laws $\sigma(w)$ that closely match the cohesive softening law from a single-size bone can differ by as much as 72.4 and 100 %. Such differences underestimate the peak loads when the size becomes $\sqrt{6}$ times smaller. Although these bilinear laws produce almost the same load–δ_{CMOD} curves as in Fig. 7a, they give different peak loads for smaller sizes (Fig. 7c). The difference between P_1 and P_2 is 16 %, which is not negligible even after taking into account the inevitable random scatter.

As a remedy, the most efficient way to identify the bilinear cohesive parameters of bovine femur is as follows:

1. Test at least three geometrically similar specimens of different sizes. The size ratios of the smallest to the largest is recommended to be at least 1:6. Specimen sizes between 4 and 24 mm are preferred.
2. Determine the initial fracture energy G_f using the size effect law (Eq. 6).
3. Determine the tensile strength f_t' by Eq. 15 with $\gamma = 0.518$.
4. Run simulations with initial values of G_f and f_t' to match the peak loads obtained by size effect tests (CoV of errors $\leq$5 %)
5. Estimate total fracture energy G_F and knee stress σ_1 from the ratios G_F/G_f and σ_1/f_t'. For example, $G_F/G_f = 2$ and $\sigma_1/f_t' = 0.1$.
6. Run the simulation to match load-δ_{CMOD} curves. Adjust the ratios G_F/G_f and σ_1/f_t' until a good optimal fit is obtained (with the CoV of errors $\leq$5 %).

2.6.1 Remedy of non-uniqueness for human and other bones

Since all bone has similar constituents, the same procedure must in principle be applicable to human bones as well. While the laboratory test of the load-displacement curve is insufficient, the combination with the size effect test would have to provide a realistic estimate of the true fracture properties. But what is the necessary size range?

Unfortunately, no size effect data are currently available for human bone. Therefore, one must rely on simulation. Computer simulation is performed with four bilinear laws, pre-determined by fitting of load-δ_{CMOD} curves (Fig. 11b). Again, the size effect law related to the cohesive crack model (Eq. 13) is plotted and only the initial part of the bilinear softening curve that is parallel to the intermediate asymptote is considered (Fig. 12).

To check the goodness of fit, the CoV of errors (root-mean-square error divided by data mean) is calculated while the intermediate asymptote is shifted up and down, with its slope remaining constant. Then, by keeping the CoV of errors <5 %, the maximum breadth of the optimum size range is obtained for all the four traction-separation laws in Fig. 13.

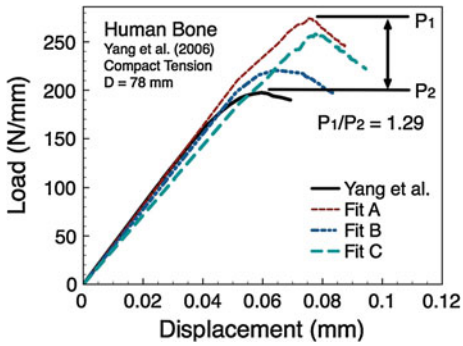

Fig. 12 Difference in peak loads when human bone size is scaled up 4 times. *Yang*, *Fit A*, *B*, and *C* represent bilinear laws from Fig. 11b

The ranges from different fits do not give the best efficiency for determining the fracture properties from the size effect data because they are too narrow and do not overlap. For example, the real size range obtained from fit C turns out to be too small, $D \in (0.035, 0.12$ mm), and it does not coincide with the others. Even after fit C is excluded, the overlapping region of the rest is $D \in (0.7, 1$ mm), which does not guarantee a sufficient size range to conduct the size effect tests.

The maximum specimen size (or beam depth) is limited by the available cortical section of the human bone, which is between 20 and 30 mm. Since the observed FPZ size in human bone is close to 5 mm (Nalla et al. 2005, 2004), the beam depths must not be smaller than that. Based on the experience with the size effect testing of concrete, beams of depth >5 mm could be used, but the testing could not be carried out with the standard equipment of mechanics of materials labs. Watchmaker-type miniaturization of testing equipment would be necessary.

Other helpful modifications to counter the size range limitations are possible. What matters for the size effect range is not the actual sizes but the dimensionless brittleness number β, which depends not only on the specimen size but also on its geometry (Bažant and Planas 1998; Bažant 2005). By testing notched beams of different depths D with notches of two relative depths, $0.15D$ and $0.50D$, it is possible to extend the range of β by almost 50 %. Furthermore, one may accept conducting the size effect tests above the aforementioned optimum size range. In that case it helps measuring the full post-peak softening load-deflection curve for each specimen and matching then all such curves by a finite element program with the cohesive crack model. Measuring not only the crack mouth opening displacement but also an opening displacement nearer the notch tip may also help.

Could it help to measure the location of the crack tip in post-peak crack propagation? Hardly. In quasibrittle materials the location of the crack tip is not precisely discernible, for two reasons: 1) there is no sharp tip but

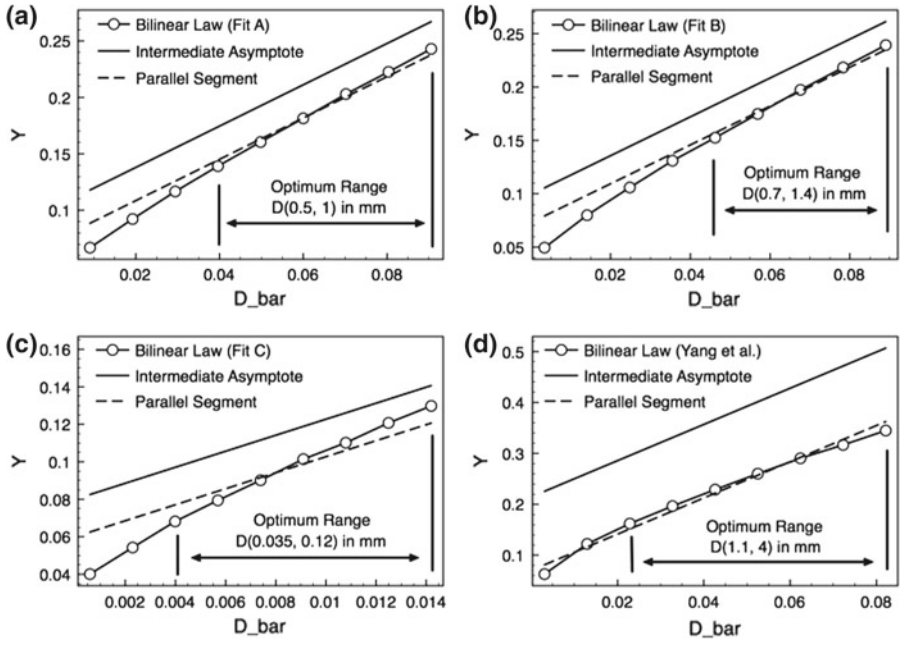

Fig. 13 Optimum size range determined from different bilinear laws of human bone. **a** Fit A, **b** Fit B, **c** Fit C, **d** Yang et al.

only a diffuse fracture process zone, and 2) the location of the crack front at mid-thickness of specimen can be very different from the location seen on the specimen surface, since the crack front is always curved. This is a problem since what matters is the crack front location averaged through the thickness.

2.7 Conclusions

1. The tests of bovine femur confirm the previous conclusion of Yang et al. (2006a,b) that fracture of bone cannot be modeled by LEFM and that the cohesive crack model is required. This means that bone is a quasibrittle material, exhibiting a size effect that is transitional between the strength theory and the LEFM.
2. The fitting of the measured complete load-defection curve of a notched specimen of only one size is not unique. In other words, such fitting is an ill-conditioned problem.
3. The load-deflection curves measured in human bone tests by Yang et al. (2006a,b) can be matched equally well with the initial fracture energy values and tensile strength values differing, respectively, by as much as 72.4 and 100 % (of the lower value).
4. The initial fracture energy, the tensile strength and the knee point coordinate of bovine as well as human bone cannot be determined by testing specimens of one size.
5. Fitting of size effect test data by Bažant's size effect law may be used to identify the initial fracture energy of the cohesive crack model of bovine as well as human bones, which is what should normally suffice to compute the strength (or load capacity) of bones and the effect of implants. Alone, however, such fitting does not suffice to determine the total fracture energy and the tail of the cohesive softening stress-separation law.
6. If the measurement of the postpeak load-deflection curve of notched specimens of one size is supplemented by size effect tests with a sufficient size range, the cohesive fracture characteristics of bone can be identified uniquely.
7. To minimize random scatter, all the specimens for size effect testing must be cut from one and the same bone. But this prevents the number of specimens from being larger than about 8. Such a small number enhances randomness of test results and is the likely explanation of a certain anomaly in the observed size effect. Alternatively, the averaging of data form a large number of specimens from many bones and many cows could be used to minimize randomness in the mean size effect.
8. Achieving a sufficient size effect range with human bone specimens in a standard mechanics of materials laboratory is difficult. The size range of the test beam depths could be extended down to millimeter-range, but a special miniaturized equipment would be needed for that. Varying the specimen geometry, e.g., by using beams of two rather different relative notch depths, could significantly extend the range of brittleness number.

Acknowledgments Partial financial support under NSF grant CMMI-1129449 to Northwestern University is gratefully acknowledged. The first author wishes to thank for partial support under W. P. Murphy Fellowship of Northwestern University.

Appendix I: Treatment of bone orthotropy and numerical simulation procedures

The bovine femur, as well as all bone, is an orthotropic material. The orthotropy has easily been taken into account in finite element computations of the dimensionless energy release rate function $g(\alpha)$ and stress intensity factor K_I.

For analytical formulation, the effective modulus based on Bao et al. (1992) was adopted. Assuming orthotropic transversely isotropic properties, one has five independent elastic constants, with the following values for the bovine femur: $E_1 = 30$ GPa, $E_2 = 15$ GPa, $G_{12} = 12.5$ GPa, $\nu_{12} = 0.206$, $\nu_{21} = 0.103$. The subscripts 1 and 2 refer to the longitudinal directions of the beam specimens and of the bone fibers (Fig. 2). According to Bao et al., the stress intensity factor can be written as:

$$K_I = \sigma\sqrt{\pi D\alpha}\,Y(\rho)F(\alpha) \tag{16}$$

where

$$\rho = \sqrt{E_1 E_2}\,/2G_{12} - \sqrt{\nu_{12}\nu_{21}} \quad \lambda = E_2/E_1 \tag{17}$$

$$Y(\rho) = \Big[1 + 0.1(\rho-1) - 0.015(\rho-1)^2 + 0.002(\rho-1)^3\Big]\,[(1+\rho)/2]^{-1/4} \tag{18}$$

$F(\alpha)$ is the same function of the relative crack length $\alpha = a/D$ as for isotropic materials. The energy release rate for an orthotropic material is:

$$G(\alpha) = \sqrt{\frac{1+\rho}{2E_1E_2\sqrt{\lambda}}}K_I^2 \tag{19}$$

Substituting Eq. (16) into (19), and changing the form as for the isotropic materials, we have

$$G(\alpha) = \frac{K_I^2}{E_{ef}} = \frac{\sigma^2 D\pi\alpha}{E_{ef}}[F(\alpha)]^2 = \frac{\sigma^2 D}{E_{ef}}g(\alpha) \tag{20}$$

where

$$E_{ef} = [Y(\rho)]^{-2}\sqrt{2E_1E_2\sqrt{\lambda}/(1+\rho)} \tag{21}$$

$$g(\alpha) = \pi\alpha[F(\alpha)]^2 = [k(\alpha)]^2 \tag{22}$$

Energy release rate $g(\alpha)$ is the dimensionless energy release function. E_{ef} is the effective modulus which is needed for formulating the size effect law (Eq. 6). For the three-point bending specimen (Tada et al. 1985):

$$k(\alpha) = \sqrt{\alpha}\frac{\begin{array}{c}1.900-\alpha[-0.089+0.603(1-\alpha)\\ -0.441(1-\alpha)^2+1.223(1-\alpha)^3]\end{array}}{(1+2\alpha)(1-\alpha)^{3/2}} \tag{23}$$

Note that, $K_I^2 = GE_{ef}$ where G = energy release rate and E_{ef} = effective Young's modulus. Then we have $g(\alpha) = \pi\alpha[F(\alpha)]^2$. The equations for $g(\alpha)$ and $g'(\alpha)$ for energy release rate at initial notch depth $0.2D$ are as follows:

$$\begin{aligned} g(\alpha) = {} & \frac{\alpha}{(1+2\alpha)^2(1-\alpha)^3}\{1.900-\alpha[-0.089\\ & +0.603(1-\alpha)-0.441(1-\alpha)^2\\ & +1.223(1-\alpha)^3]\}^2 \end{aligned} \tag{24}$$

Finally $g'(\alpha_0)$ can be obtained through numerical differentiation.

Appendix II: Comparison with human bone examples Yang et al. (2006a, b)

Using finite elements, the softening load-deflection curves of human bone, reported in Yang et al. (2006a,b), are reproduced in Figs. 8 and 11 using the following parameters:

$$f_t' = p_c = 60\ \text{MPa}, \quad w_c = u_c = 36\ \mu\text{m},$$
$$\sigma_1 = p_0 = 30\ \text{MPa}, \quad w_1 = u_0 = 6\ \mu\text{m} \tag{25}$$

$$W_{tip} = 0.544\ \text{kJ/m}^2, \quad W_{brid} = 0.90\ \text{kJ/m}^2 \tag{26}$$

Yang's bilinear values were varied to fit data scatter. For example, they assumed that p_c has the mean, 60 MPa and standard error, 10 MPa (60 ± 10 MPa).

According to Fig. 1, our definition of G_f is the area of the triangle under the initial straight softening segment. On the other hand, W_{tip} is area of trapezoids according to Yang's definition. To interpret results in terms of G_f, W_{tip} must be converted to G_f or otherwise the initial fracture energy could be underestimated since $G_f > W_{tip}$. After conversion, the initial fracture energy of Yang's bilinear law G_f becomes $0.72\ \text{kJ/m}^2$.

The total fracture energy, G_F, for Yang et al.'s tests can be calculated by adding W_{tip} to W_{brid},

$$G_F = W_{tip} + W_{brid} = 0.544 + 0.90 = 1.44\ \text{kJ/m}^2 \tag{27}$$

References

Bao G, Ho S, Suo Z, Fan B (1992) The role of material orthotropy in fracture specimens for composites. Int J Solids Struct 29(9):1105–1116

Barenblatt GI (1959) The formulation of equilibrium cracks during brittle fracture, general ideas and hypothesis, axially symmetric cracks. Prikl Mat Mech 23(3):434–444

Barenblatt GI (1962) The mathematical theory of equilibrium of cracks in brittle failure. Adv Appl 7:55–129

Bažant ZP (1984) Size effect in blunt fracture: concrete, rock, metal. J Eng Mech ASCE 110(4):518–535

Bažant ZP (1997) Scaling theory for quasibrittle structural failure. Proc Natl Acad Sci USA 101(37):13400–13407

Bažant ZP (2005) Scaling of structural strength. Elsevier, London

Bažant ZP, Becq-Giraudon E (1999) Effects of size and slenderness on ductility of fracturing structures. J Eng Mech ASCE 125(3):331–339

Bažant ZP, Kazemi MT (1990) Determination of fracture energy, process zone length, and brittleness number from size effect, with application to rock and concrete. Int J Fract 44:111–131

Bažant ZP, Kazemi MT (1991) Size effect on diagonal shear failure of beams without stirrups. ACI Struct J 88(3):268–276

Bažant ZP, Planas J (1998) Fracture and size effect in concrete and other quasibrittle materials. CRC Press, Boca Raton

Bažant ZP, Oh B-H (1983) Crack band theory for fracture of concrete. Mater Struct 16(3):155–177

Bažant ZP, Yu Q (2011) Size-effect testing of cohesive fracture parameters and nonuniqueness of work-of-fracture method. J Eng Mech ASCE 137(8):580–588

Cusatis G, Schauffert EA (2009) Cohesive crack analysis of size effect. Eng Fract Mech 76(14):2163–2173

Guinea GV, Planas J, Elices M (1992) Measurement of the fracture energy using 3-point bend tests. 1. Influence of experimental procedures. Int J Fract 138:101–137

Hillerborg A, Modéer M, Petersson PE (1976) Analysis of crack formation and crack growth in concrete by means of fracture mechanics and finite elements. Cem Concr Res 6(6):773–782

Irwin GR (1958) Fracture. In: Flügge (ed) Handbuch der Physik. Springer, Berlin, vol 6, pp 551–590

Nakayama J (1965) Direct measurement of fracture energies of brittle heterogeneous materials. J Am Ceram Soc 48(11):583

Nalla RK, Kruzic JJ, Ritchie RO (2004) On the origin of the toughness of mineralized tissue: micro cracking or crack bridging? Bone 34(5):790–8

Nalla RK, Kruzic JJ, Kinney JH, Ritchie RO (2005) Mechanistic aspects of fracture and R-curve behavior in human cortical bone. Biomaterials 26(2):217–31

Petersson PE (1981) Crack growth and development of fracture zones in plain concrete and similar materials. Report TVBM-1006 (Dissertation), Div. of Building Materials, Lund Inst. of Technol., Lund, Sweden

RILEM (1990) Size-effect method for determining fracture energy and process zone size of concrete. Mater Struct 23:461–465

Rokugo K, Iwasa M, Suzuki T, Koyanagi W (1989) Testing methods to determine tensile strain softening curve and fracture energy of concrete. In: Mihashi H, Takahashi H, Wittmann FH (eds) Fracture toughness and fracture energy: test methods for concrete and rock. Balkema, Rotterdam, pp 153–163

Tada H, Paris PC, Irwin GR (1985) The stress analysis of cracks handbook, 2nd edn. Paris Productions Inc., MO

Tattersall HG, Tappin G (1966) The work of fracture and its measurement in metals, ceramics and other materials. J Mater Sci 1(3):296–301

Van Buskirk WC, Cowin SC, Ward RN (1981) Ultrasonic measurement of orthotropic elastic constants bovine femoral bone. J Biomech Eng 103:67–72

Yang QD, Cox BN, Nalla RK, Ritchie RO (2006a) Fracture length scales in human cortical bone: necessity of nonlinear fracture models. Biomaterials 27:2095–2113

Yang QD, Cox BN, Nalla RK, Ritchie RO (2006b) Re-evaluating the toughness of human cortical bone. Bone 38(6):878–887

Yu Q, Le Jia-liang, Hoover CG, Bažant ZP (2010) Problems with Hu-Duan boundary effect model and its comparison to size-shape effect law for quasi-brittle fracture. J Eng Mech ASCE 136(1):40–50